ORIGINAL ARTICLE

High throughput static and dynamic small animal imaging using clinical PET/CT: potential preclinical applications

Nicolas Aide · Cédric Desmonts · Jean-Mathieu Beauregard · Thomas Beyer ·
Kathryn Kinross · Peter Roselt · Oliver Neels · Denis Agostini · Stéphane Bardet ·
Gérard Bouvard · Rodney J. Hicks

Abstract

Purpose The objective of the study was to evaluate state-of-the-art clinical PET/CT technology in performing static and dynamic imaging of several mice simultaneously.

Methods A mouse-sized phantom was imaged mimicking simultaneous imaging of three mice with computation of recovery coefficients (RCs) and spillover ratios (SORs). Fifteen mice harbouring abdominal or subcutaneous tumours were imaged on clinical PET/CT with point spread function (PSF) reconstruction after injection of [18F]fluorodeoxyglucose or [18F]fluorothymidine. Three of these mice were imaged alone and simultaneously at radial positions –5, 0 and 5 cm. The remaining 12 tumour-bearing mice were imaged in groups of 3 to establish the quantitative accuracy of PET data using ex vivo gamma counting as the reference. Finally, a dynamic scan was performed in three mice simultaneously after the injection of ^{68}Ga-ethylenediaminetetraacetic acid (EDTA).

Results For typical lesion sizes of 7–8 mm phantom experiments indicated RCs of 0.42 and 0.76 for ordered subsets expectation maximization (OSEM) and PSF reconstruction, respectively. For PSF reconstruction, SOR$_{air}$ and SOR$_{water}$ were 5.3 and 7.5%, respectively. A strong correlation ($r^2=0.97$, $p<0.0001$) between quantitative data obtained in mice imaged alone and simultaneously in a group of three was found following PSF reconstruction. The correlation between ex vivo counting and PET/CT data was better with PSF reconstruction ($r^2=0.98$; slope=0.89, $p<0.0001$) than without ($r^2=0.96$; slope=0.62, $p<0.001$). Valid time-activity curves of the blood pool, kidneys and bladder could be derived from ^{68}Ga-EDTA dynamic acquisition.

N. Aide
Bioticla Team, EA1792, IFR 146 ICORE, GRECAN,
François Baclesse Cancer Centre and Caen University,
Caen, France

N. Aide · C. Desmonts · D. Agostini · S. Bardet · G. Bouvard
PET Unit, Caen University Hospital
and François Baclesse Cancer Centre,
Caen, France

N. Aide · J.-M. Beauregard · K. Kinross · P. Roselt · O. Neels ·
R. J. Hicks
Centre for Molecular Imaging, Peter MacCallum Cancer Centre,
East Melbourne, Australia

T. Beyer
cmi-experts GmbH,
Zurich, Switzerland

T. Beyer
Department of Nuclear Medicine, University Hospital Essen,
Essen, Germany

T. Beyer
Institute of Nuclear Medicine, University Hospital Bern,
Bern, Switzerland

K. Kinross
Sir Donald and Lady Trescowthick Laboratories,
Peter MacCallum Cancer Centre,
East Melbourne, Australia

R. J. Hicks
The Department of Medicine, University of Melbourne,
Parkville, Australia

N. Aide (✉)
Nuclear Medicine Department, Centre François Baclesse,
Avenue Général Harris,
14076 Caen cedex 5, France
e-mail: n.aide@baclesse.fr

Conclusion New generation clinical PET/CT can be used for simultaneous imaging of multiple small animals in experiments requiring high throughput and where a dedicated small animal PET system is not available.

Keywords Molecular imaging · PET/CT · PSF reconstruction · Cancer research · Preclinical studies

Introduction

Immunodeficient rodents bearing xenografted human tumours and transgenic mice bearing spontaneous tumours are the cornerstone of oncological preclinical models. Dedicated small animal positron emission tomography (DSA PET) is a powerful means for preclinical studies involving such tumour/disease models. DSA PET are used for tumour take rate evaluation [1] and early evaluation of treatment based on either conventional chemotherapy [2] or inhibitors of the tumour transduction signal [3].

Typically, small animal PET imaging is performed on DSA PET systems. However, these dedicated imaging devices are less widely available than clinical PET and PET/CT. Therefore, researchers have tried to image small rodents on clinical PET systems [4]. A major limitation of clinical PET imaging technology is the limited spatial resolution that—in the context of small animal imaging—degrades significantly with the radial distance from the centre of the field of view (FOV).

However, recently new advanced reconstruction algorithms that model the point spread function (PSF) of individual detector elements have become commercially available in clinical PET/CT [5–7]. Based on the implemented PSF reconstruction the spatial resolution of PET/CT has improved and approaches those of earlier generation DSA PET [8]. Therefore, new generation clinical PET/CT could, in theory, be useful to image mice bearing tumours, in contrast with clinical PET/CT equipped with classic iterative reconstruction methods, for which murine imaging is not feasible because of significant partial volume effect [9].

In cancer research, the number of animals that require imaging is potentially high. However, the number of animals that can be imaged within a DSA PET session is limited by the relatively long procedure, which may take 20 min per animal if a separate transmission scan is performed for attenuation correction [10]. Therefore, being able to image several animals simultaneously would be extremely valuable, allowing a dramatic increase in scanning throughput. New generation clinical PET/CT equipped with PSF reconstruction have a large FOV (70 cm) and good spatial resolution throughout the entire

FOV. Therefore, degradation of image quality would not be anticipated when imaging several mice simultaneously.

This study aims to evaluate the ability of a new generation clinical PET/CT scanner to perform both static and dynamic preclinical imaging of small animals with a focus on its capability to image several rodents simultaneously.

Materials and methods

Clinical PET/CT system

All PET imaging studies were performed on a Biograph TrueV (Siemens Healthcare). Phantom studies were performed at the PET unit of the François Baclesse Cancer Centre/University Hospital of Caen using the TrueV 6 (with a 6-slice spiral CT component). Animal examinations were performed at the Centre for Molecular Imaging of the Peter MacCallum Cancer Centre with a TrueV 64. Table 1 summarizes the technical and performance characteristics of the PET components of the TrueV system.

Tracer synthesis

[18F]Fluorodeoxyglucose (^{18}F-FDG) was purchased from Cyclotek (Melbourne, Australia) or Cyclopharma (Saint-Beauzire, France). 3′-Deoxy-3′-[18F]fluorothymidine (^{18}F-FLT) was prepared at the Peter MacCallum Cancer Centre

Table 1 TrueV Biograph PET/CT (Siemens Healthcare): PET system and performance characteristics

Characteristic	Value for the TrueV Biograph
Detector ring diameter (cm)	84.2
Detector material	LSO
No. of individual crystals	32,448
No. of crystals per ring	624
No. of detector rings	52
No. of image planes per bed position	109
Crystal size (mm^3)	4×4×20
No. of detector blocks	192
Patient port diameter (cm)	70
Axial FOV (cm)	21.6
Transaxial FOV (cm)	60.5
NECR	165 kcps @ 32 kBq/ml[a]
Sensitivity	7.9 cps/kBq @ 425 keV[a, b]

LSO lutetium orthosilicate, *NECR* noise equivalent count rate

[a] Values quoted by manufacturer

[b] The sensitivity of the Inveon state-of-the-art small animal PET is 29.35 cps/kBq for an energy window of 350–650 keV and coincidence window of 3.4 ns [33]

on the GE Tracerlab FXFN module using the method described by Machulla et al. [11].

For ^{68}Ga-ethylenediaminetetraacetic acid (EDTA) synthesis performed at the Peter MacCallum Cancer Centre, a commercial [68]Ge/^{68}Ga generator was obtained from IDB Holland BV (Barle-Nassau, The Netherlands). [68]Ga was eluted from the generator using 0.5 N HCl and purified as described by Zhernosekov et al. [12]. The purified ^{68}Ga was eluted into 5 ml Milli-Q water containing 0.1 mg disodium EDTA and reacted at 120° for 10 min. The final product solution was filtered using a Millex-GV filter (Millipore).

Phantom studies

Determination of spatial resolution of the clinical PET/CT system

Spatial resolution of the PET/CT was determined by imaging point sources placed in air at different radial offsets in the centre of the FOV. Point sources were made of capillary tubes of 0.5 mm inner diameter filled with a 70 MBq/ml solution of ^{18}F-FDG. Full-width at half-maximum (FWHM) PSF was determined in the radial direction, along profiles passing through the distribution peak, as recommended by the National Electrical Manufacturers Association (NEMA) NU-2001 standard [13, 14].

Phantom experiment for recovery coefficients (RCs) and spillover ratios (SORs)

A Micro-Deluxe phantom (Data Spectrum Corporation) was used to study RCs and SORs for the clinical PET. This phantom consisted of a main chamber (internal diameter 4.5 cm, external diameter 5 cm), containing either fillable spheres or two small cylinders. Diameters of the fillable spheres were: 3.95, 4.95, 6.23, 7.86 and 9.89 mm, and their centres were located within a single transaxial plane. Inner diameter and length of the cylinders used to compute the SOR were 10 and 20 mm, respectively.

In order to study RCs, the main chamber and the spheres were filled with an ^{18}F-FDG solution with a background activity of 0.46 MBq/ml and a sphere to background ratio of 5. For the evaluation of SORs, the main chamber was filled with the same background activity (0.46 MBq/ml), while one cylinder was filled with non-radioactive water and the other kept empty (air-filled).

In all experiments the phantom was fixed on a flat carbon fibre radiotherapy table. First, the lesion phantom was imaged at 0 cm (centre FOV) and at 5 cm (radial offset). This offset corresponds to the position of a mouse if three animals were to be imaged simultaneously, i.e. one mouse at the FOV centre with two mice on either side.

Second, the cylinder phantom was imaged in the presence of two cylindrical ^{18}F-FDG sources, to simulate the simultaneous presence of three rodents in the FOV and evaluate the impact on image quality of attenuation and scatter radiation due to multiple rodents. The lesion phantom was placed at −5 cm and the two activity sources at 0 and +5 cm radially.

In all imaging sessions the CT acquisition was performed first with: 80 mAs, 130 kVp, pitch 1 and 6×1 mm collimation. Subsequently, the PET static emission acquisition was performed in 3-D mode. For each phantom (or group thereof), the duration of the first acquisition was 20 min and the duration of subsequent acquisitions was increased to account for ^{18}F decay. PET images were reconstructed with a zoom of 2 (reconstructed FOV= 35 cm) and two different algorithms. First, a standard ordered subsets expectation maximization (OSEM) 3-D reconstruction algorithm with 4 iterations and 8 subsets was used. Second, the PSF reconstruction algorithm (HD; TrueX, Siemens Medical Solutions) with 6 iterations and 16 subsets was used. In both reconstruction modes the matrix size was 336^2, resulting in a $1.02 \times 1.02 \times 1$ mm^3 voxel size. Scatter [15] and attenuation corrections [16] were applied prior to image reconstruction.

Animal studies

Small animal models

Animal studies were performed with approval of the Peter MacCallum Cancer Centre Animal Ethics Committee. A total of 18 mice were used of which 15 were tumour-bearing mice. These 18 mice comprised 5 separate experimental groups. These were a genetically engineered murine model [Lox-Stop-Lox (LSL) Kras$^{G12D/+}$/Pten$^{fl/fl}$] [17] that develops spontaneous orthotopic ovarian cancers ($n=3$) and nude mice with transplanted ovarian cancers ($n=6$) or subcutaneous xenografts of prostate cancer (PC3 tumours, $n=3$) or ovarian cancer (SKOV-3 tumours, $n=3$). Three nude mice without tumour were used for a dynamic study.

Static PET/CT imaging of mice

All animals fasted for 3 h prior to imaging. Tracer injection was performed via the tail vein with a solution of ^{18}F-FDG (16–32 MBq in 0.1–0.2 ml) and ^{18}F-FLT (32–37 MBq in 0.1 ml) in six animals each. In six PET/CT examinations (three ^{18}F-FDG and three ^{18}F-FLT) an intravenous (IV) contrast media agent was co-injected (eXia 160XL, Benitio International, Canada). eXia 160XL is an aqueous colloidal polydisperse contrast agent, which avoids renal filtration and diffusion from the intravascular into the interstitial space, thereby

providing long-lasting vascular enhancement, together with splenic and liver enhancement. This contrast media was mixed with the radiotracer, in order to perform only one tail vein injection per animal. The total volume of the injection was always kept below 0.2 ml. To minimize muscle and brown fat uptake in the case of ^{18}F-FDG imaging, animals were kept anaesthetized under warming lights for a 20-min period after injection. Animals were sacrificed 45–60 min after injection to minimize changes in biodistribution between consecutive imaging sessions and ex vivo counting.

Single versus multiple animal static imaging comparison

First, three animals injected with ^{18}F-FDG were imaged simultaneously in the FOV of the PET/CT at –5, 0 and +5 cm (radial) and then, one by one at the centre of the FOV (0 cm). A total of 15 tumours and organs in these 3 mice were used for quantitative analysis. This procedure was designed to assess the impact of the radial offset and of the presence of multiple animals in the FOV of the PET/CT scanner on image quality and accuracy of quantitative measurements.

Accuracy of static imaging in multiple animals

Animals were injected with ^{18}F-FLT ($n=6$) and ^{18}F-FDG ($n=6$) and were imaged simultaneously in groups of three on the PET/CT. A total of 27 tissue samples (9 tumours, 18 organs) were used for quantitative analysis.

PET/CT imaging parameters

CT acquisition was performed first with the following parameters: 80 mAs, 130 kVp, pitch 1 and 64×0.6 mm collimation. Subsequently, the PET static emission acquisition was performed in 3-D mode. For each animal (or group thereof), the duration of the first acquisition was 10 min. For the single versus multiple animal static imaging comparison, when the animal was imaged more than once on the PET/CT, the duration of subsequent acquisition was increased to account for ^{18}F decay.

PET images were reconstructed with the same parameters used for reconstruction of the phantom studies.

Ex vivo counting

Immediately after the static PET examination had been performed, tumours and organs were harvested. Tissue samples were weighed with a precision scale (±0.01 mg). Tumour radioactivity was counted for 1 min in a cylinder well counter (Wallac 1470 automatic gamma counter) and corrected for instrument efficiency and decay. Counts per minute were converted to Bq and normalized for sample weight, assuming a density of 1 g/ml.

Dynamic ^{68}Ga-EDTA PET/CT study

For the dynamic scan, a cannula was placed in the tail vein of three mice under general anaesthesia, which was performed using a mixture of ketamine and xylazine. One mouse was placed at the centre of the FOV and the other two were placed on each side of the central animal, at a 5-cm radial offset to the left and right. The three mice were injected sequentially, within a 1.5-min period, with a solution of ^{68}Ga-EDTA (40 MBq in 0.1 ml). Immediately after the tracer injection, the cannula was flushed with 0.1 ml of normal saline. The dynamic emission acquisition was started immediately before the first injection and continued for a duration of 20 min. Data were stored in list mode and then reframed as follows: 10 frames of 30 s, followed by 15 frames of 60 s. PET images were reconstructed with the same parameters used for reconstruction of the phantom studies.

Data analysis

Phantom studies

RCs, defined as the ratio between measured and true activity [18, 19], and previously used in small animal PET phantom imaging [20], were computed using planar regions of interest (ROI). Planar ROI were defined manually in the image plane with the largest lesion diameter. Plots of RC against sphere diameters were obtained and curves were then fitted to obtain RC as a function of sphere diameters.

SORs were computed as the ratio between activity in the water-filled and air-filled cylinders and the real activity. Activity in the cylinders was obtained by drawing a cylindrical volume of interest (VOI) with a diameter half the physical diameter of the cylinders (5 mm) and a length of 10 mm.

Static animal studies

Tumour activity was obtained in each static image volume from a VOI encompassing the entire lesion or organ. VOIs were defined by using an isocontour threshold method to obtain concordance between the measured tumour volume on PET and CT images. When discordance was encountered between PET metabolic volume and CT volume, the VOI was adjusted to match the CT volume. This enabled PET/CT images to be compared to ex vivo counting in which the entire tumour was harvested and analysed independent of the potential presence of non-viable areas. Additionally, tumour to background ratios (T/B ratios) were obtained by dividing the VOI value of the tumour by the activity of a planar ROI placed in the abdomen, in the vicinity of the tumour but excluding areas of increased uptake such as the kidneys.

For evaluation of quantitative accuracy, the relationship between the concentration of radioactivity in animal images

and tissue samples, as determined by clinical PET/CT and by gamma counter, respectively, was assessed using a linear regression analysis. In addition to regression analysis, Bland-Altman plots were constructed [21, 22]. The same analysis was conducted to correlate the uptake values in the same mouse lesions and organs when imaged alone versus in a group. T/B ratios were compared for OSEM 3-D and PSF reconstruction using the Wilcoxon test for paired samples. A two-tailed p value of 0.05 was considered statistically significant.

Dynamic animal studies

For the dynamic acquisition, ROIs were drawn on a single transverse slice on the heart, one kidney and the bladder. The ROIs (3×3 mm) were centred on the pixel harbouring the highest activity value and then copied automatically on all other time frames of that slice. Time-activity curves (TACs) were then generated and assessed.

Results

Phantom studies

Point source resolution following OSEM 3-D reconstruction was 4.17 mm (FWHM) at 0 cm (centre FOV) and deteriorated to 5.37 mm at a 15-cm radial offset. Spatial resolution was better with PSF reconstruction: 2.09 mm and =3 mm at 0- and 15-cm radial offset, respectively (Fig. 1a).

For a centrally positioned phantom, the RC for the three largest spheres were lower for images reconstructed with the OSEM 3-D algorithm than for those following PSF reconstruction. For the two smallest spheres the RC decreased significantly for both reconstruction methods although the PSF reconstruction still leads to slightly higher RC values (Fig. 1c, d).

Still, the RCs for the 7.86-mm sphere, which represents a common lesion size in mice bearing subcutaneous tumours [23, 24], were 0.42 for OSEM reconstruction and 0.76 for PSF reconstruction when the phantom was imaged in an off-centred position together with two additional sources. For this lesion, the percentage of variation between RC values for an off-centred acquisition, compared to centred acquisition, was −2.3% in the presence of additional scatter and attenuation sources and −1.1% in the case of a single phantom imaged in the central FOV.

SORs for the water-filled and air-filled cylinders were 4.4 and 6%, respectively. When imaging two additional sources to mimic scatter events introduced when imaging three mice simultaneously, SORs increased to 5.3% in water and 7.5% in air. In contrast, when images were reconstructed with OSEM 3-D SORs were greater than 13% (Fig. 1b).

Fig. 1 FWHM of the PSF of point sources imaged in air following OSEM 3-D algorithm and PSF reconstruction (**a**). SOR, defined as the activity ratio in air- and water-filled cylinders (10 mm in diameter) versus surrounding activity (**b**). RCs defined as the ratio of measured and true activity concentration as a function of sphere diameters following OSEM 3-D and PSF reconstruction (**c**, **d**). Phantom data are given for phantoms placed either at the centre of the FOV or at a 5-cm radial offset and imaged without or with additional cylindrical sources mimicking multiple rodents
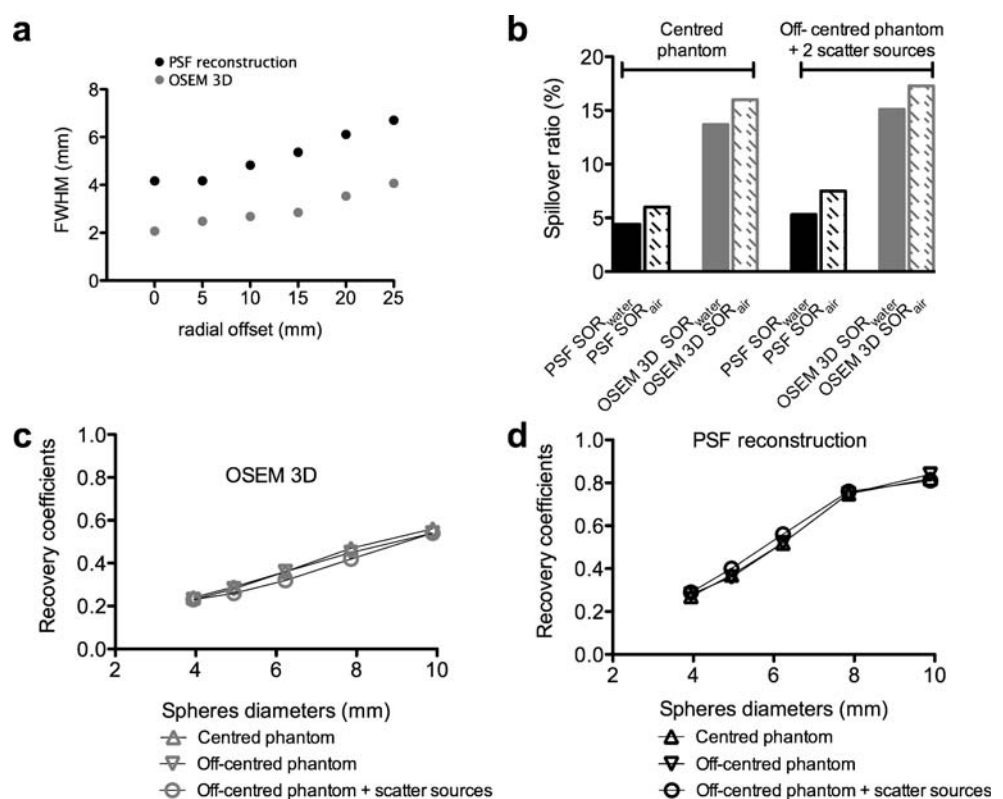
Static PET/CT: single versus multiple animal static imaging comparison

An excellent correlation (r^2=0.97) was found between quantitative measurements performed on mice that were centred in the FOV and those when mice had been imaged simultaneously within a group of three (Fig. 2a). Bland-Altman analysis also demonstrated that the mean ratio between off-centred quantitative measurements and centred quantitative measurements was close to 1 with narrow 95% limits of confidence (Fig. 2b).

Static imaging in multiple animals

The mean weight of tissue samples used for quantification was 0.22 g (range: 0.08–0.45 g). The smallest detected tumour was less than 4 mm in size (Fig. 3). Correlation of radioactivity concentration in animal lesions, as determined by clinical PET and by ex vivo counting, was good for OSEM 3-D reconstruction (r^2=0.93) and somewhat better for PSF reconstruction (r^2=0.97) (Fig. 4a, c). Bland-Altman analysis demonstrated that the mean ratio between ex vivo quantitation and clinical PET quantitation was better with PSF reconstruction (Fig. 4b, d). PSF reconstruction improved T/B ratios (2.4 ± 0.9, p=0.004) as compared to OSEM 3-D (1.4 ± 0.3). Figure 5 shows fused maximum intensity projection (MIP) and a coronal section of three mice bearing ovarian tumours imaged simultaneously. The

Fig. 2 Linear regression analysis (**a**) shows a strong correlation (r^2= 0.97). Bland-Altman graph (**b**) shows a ratio between quantitative data for centred and off-centred mice close to unity with narrow 95% confidence limits

CT component of the PET/CT acquisition was used for attenuation correction purposes but also allowed a better localization of the areas of increased tracer uptake, especially in the case of abdominal tumours. In the Lox-Stop-Lox (LSL) Kras$^{G12D/+}$/Pten$^{fl/fl}$ mice, which tend to have more abdominal fat than the nude mice, visualization of the ovarian tumours was particularly easy, thanks to the fatty areas around them, which appeared as low densities in contrast to the tumours, which are of tissular density (Fig. 5). In nude mice, which lack abdominal fat, image quality was poorer, especially in the case of haemorrhagic ascites (Fig. 3f).

Dynamic, simultaneous ^{68}Ga-EDTA PET/CT imaging of three mice

PET images were of good quality and no misregistration was observed between PET and CT slices. TACs were obtained from ROIs drawn over the heart, kidneys and bladder in each mouse (Fig. 6). The symmetrical nature of the TAC over each kidney and having a shape that would be expected of an excretory renogram suggests that quantitative, dynamic PET scanning might be feasible in mice using human scanners.

Discussion

Brix et al. [25] first described the implementation of a PET system model in the process of iterative image reconstruction when imaging small animals in a clinical PET system. The authors demonstrated significant improvements in the spatial resolution at the centre of the FOV when employing the derived spatial variances of the line spread function during image reconstruction. The feasibility of imaging rodents with a clinical PET, taking ex vivo counting as a reference standard, was later described by Tatsumi et al. [9] using a General Electric Discovery LS tomograph with a 5-mm spatial resolution. They showed that imaging tumours was feasible in rats and rabbits. Tumour image quality in mice was lower because of their smaller size and PSF reconstruction was not commercially available at that time. As stated by the authors, imaging mice bearing larger tumours would not have been physiologically relevant. The findings of Tatsumi et al. [9] were later confirmed by Seemann et al. [26] who compared quantitative data of mice bearing a tumour imaged on a Siemens Biograph PET/CT and on a DSA PET (Mosaic, Phillips Medical System). They found that tumours had a 1.89 higher mean T/B ratio for the DSA PET than for the PET/CT, suggesting significant partial volume effects related to the inferior spatial resolution of the clinical PET/CT. More recently, clinical PET with classic iterative reconstruction algorithms
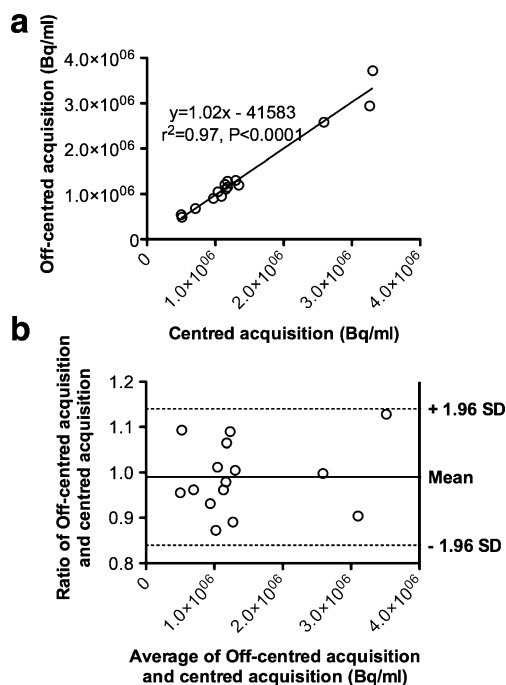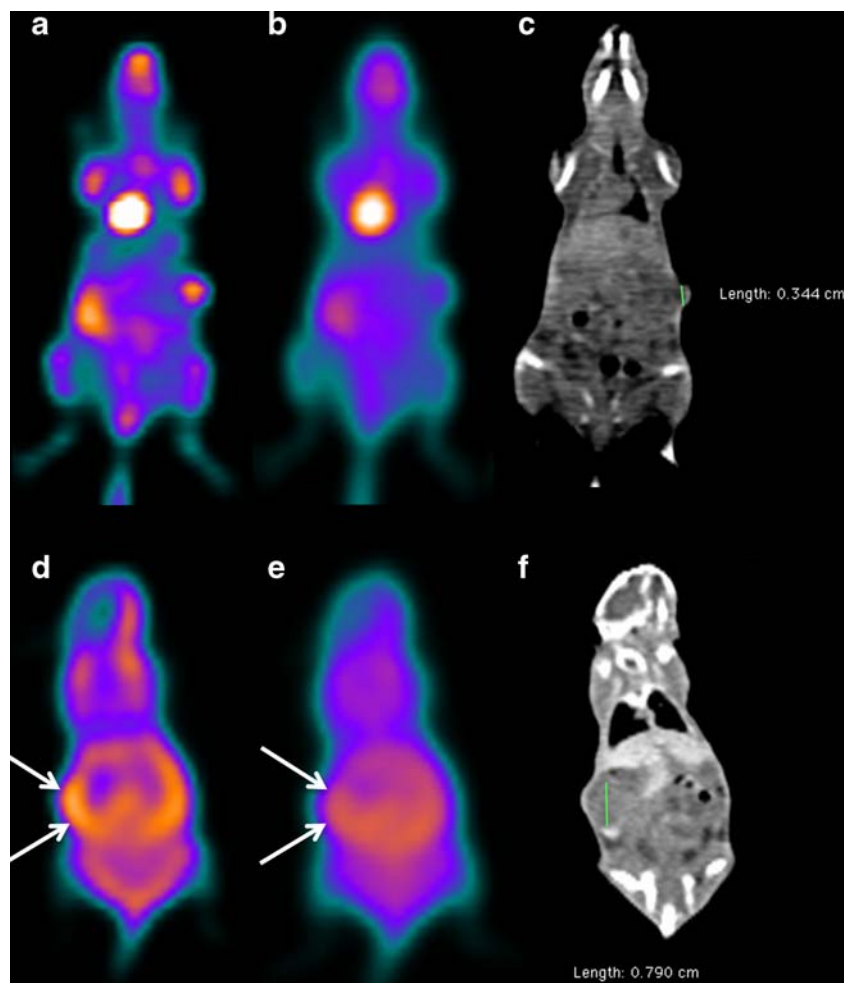
Fig. 3 Coronal slices for PET (**a**, **d**: PSF reconstruction; **b**, **e**: OSEM algorithm) and CT image (**c**, **f**) are shown for a mouse bearing subcutaneous tumour and imaged with ^{18}F-FDG and for a mouse with an ovarian tumour involving the spleen and imaged with ^{18}F-FLT. PET slices have been scaled to the same maximum. Note the improvement in T/B ratio when PSF reconstruction is used (**a**, **d**)

were used to detect head and neck tumours in rats [27] or to perform an early therapy assessment with ^{18}F-FDG in rabbits bearing subcutaneous tumours [28]. However, neither study addressed the possibility of imaging several animals simultaneously.

In our study we used state-of-the-art clinical PET/CT technology equipped with an advanced PSF reconstruction algorithm to accurately quantify radioactivity concentration within small lesions and to image several mice simultaneously. More specifically, we used ex vivo gamma counting of lesions as a reference standard and we performed simultaneous animal imaging for both static and dynamic acquisition schemes.

Thanks to advanced reconstruction algorithms, new generation clinical PET scanners display good spatial resolution throughout the entire axial FOV [6], in contrast with the decreased spatial resolution usually observed as radial offset increases. Consequently, new clinical PET devices theoretically allow several animals to be imaged at the same time with a similar image quality, regardless of the position of the animal in the FOV. Several animals can be

imaged simultaneously, given the large axial and transverse FOV of 21.6 and 60.5 cm, respectively, of clinical PET/CT technology used in the present study.

Here, we showed that imaging three mice simultaneously was feasible when using a clinical PET/CT with resolution recovery reconstruction, as no difference in image quality and quantitative accuracy was observed when the same mouse was imaged alone in the centre of the FOV or off-centre with two other mice in the FOV (Fig. 2). Excellent correlation between clinical PET/CT quantitative data reconstructed with the PSF reconstruction algorithm and ex vivo counting was found when imaging three mice simultaneously (Fig. 4).

Phantom studies (Fig. 1) showed good RC values for a 7.86-mm sphere, which represents a common lesion size in mice bearing subcutaneous tumours [23, 24]. RC degrades for very small lesions with only a minor benefit for PSF reconstruction as shown in Fig. 1. Also, SORs were altered by the presence of additional scatter sources in the FOV. Taken together, these results suggest that clinical PET/CT with PSF reconstruction should be restricted to mice model

Fig. 4 Linear regression analysis shows a marked improvement of the slope when data were reconstructed with PSF reconstruction algorithm (**c**) compared to the OSEM algorithm (**a**). Bland-Altman plot shows better ratios and 95% confidence limits between quantitative data and ex vivo counting when PSF reconstruction was used (**d**) compared to the OSEM algorithm (**b**)
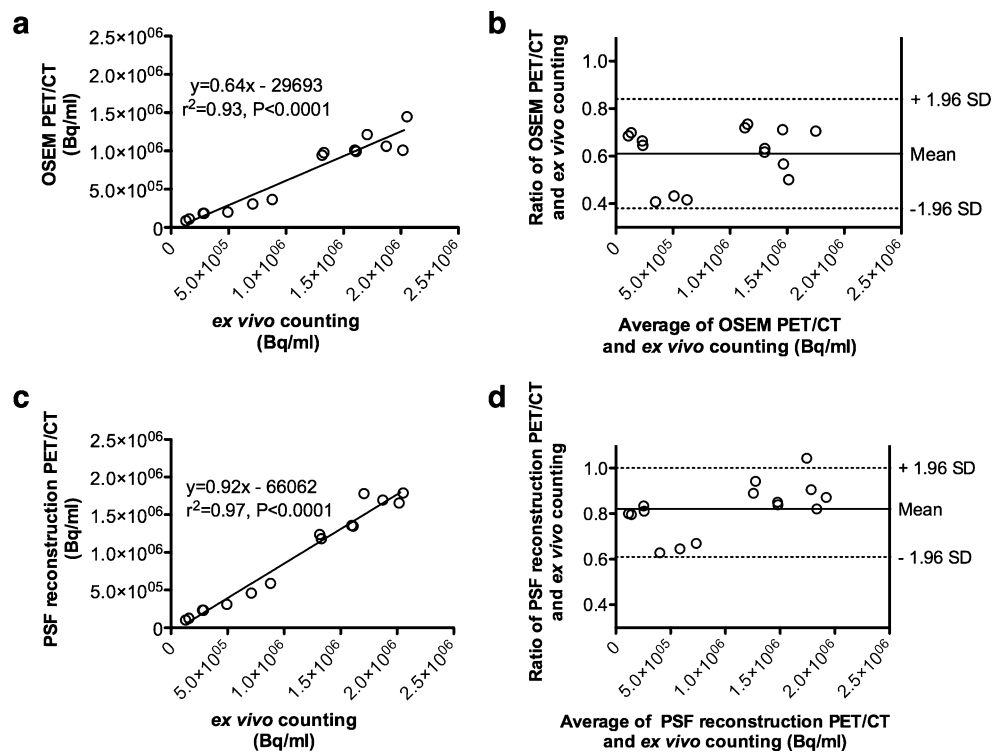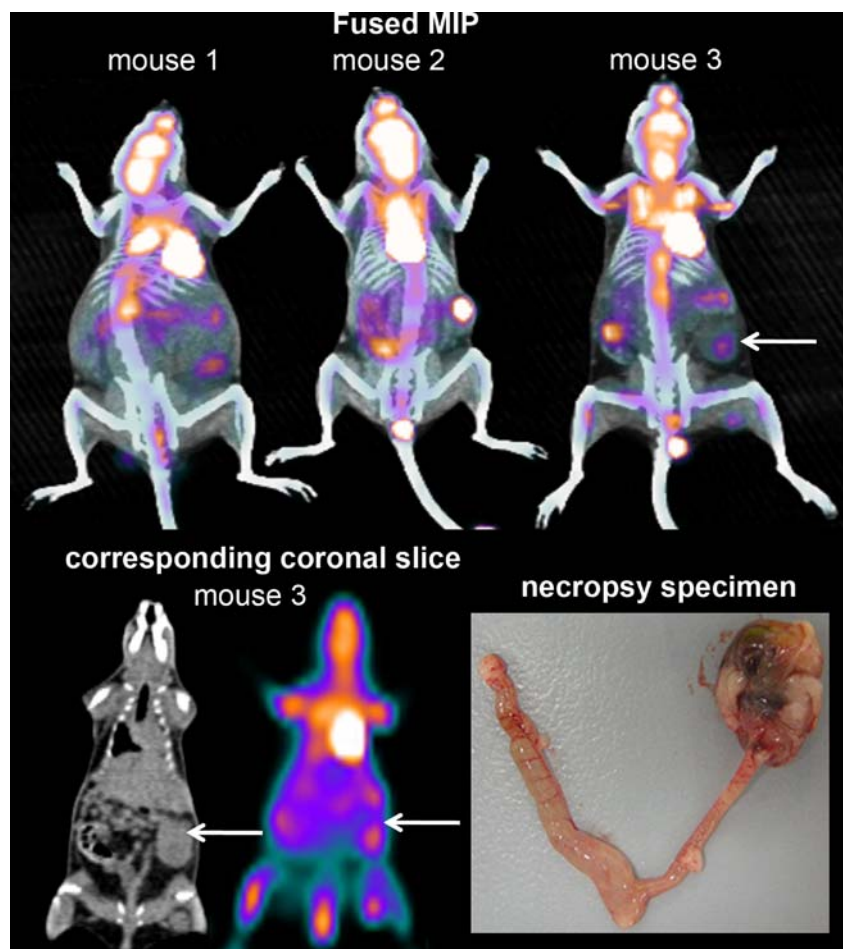

Fig. 5 Three mice bearing spontaneous left ovary tumours were imaged on the clinical PET/CT. A fused MIP picture of the three mice imaged simultaneously (mouse 1, 2 and 3 at radial offset = −5, 0 and +5 cm) is shown together with selected coronal PET (PSF reconstruction) and CT slices and the necropsy specimen of one of these mice (*white arrow*)
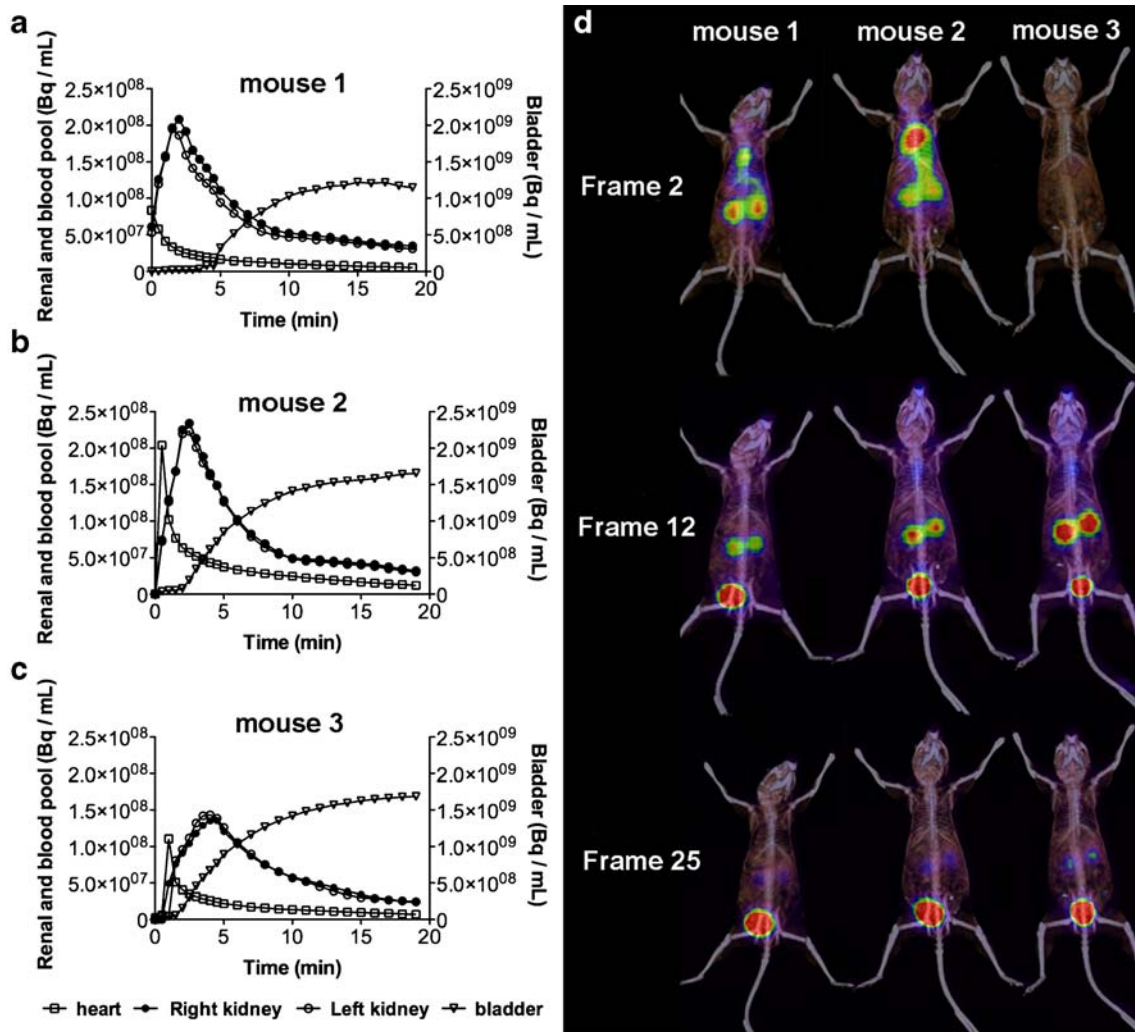
Fig. 6 A group of three mice was injected with ^{68}Ga-EDTA within a 1.5-min period. Animals were scanned for 20 min. TACs derived from ROIs drawn on one kidney, the heart and the bladder are displayed (**a** mouse 1, **b** mouse 2, **c** mouse 3). Fused PET/CT MIP pictures of an early, mid and late frame are shown in **d**. Note the progressive clearance of activity from the blood, followed by the kidneys and appearance of activity in the bladder as well as the ability to evaluate the symmetry of uptake and clearance from each kidney

with tumours >7 mm and that other studies like ^{18}F-FDG brain studies of small structures may not provide accurate quantitative data, because of a significant partial volume effect and spillover effect from areas with intense uptake, such as the harderian glands.

Our study supports the use of new generation clinical PET/CT for imaging mice as part of preclinical cancer research programmes that do not have access to a DSA PET. The possibility of simultaneous imaging of several rodents may lead to a significant improvement in imaging throughput. In our study a 10-min acquisition time was sufficient to examine three mice with a clinical PET/CT. This compares to 45–60 min for the same workload with only a DSA PET available if transmission-based attenuation correction is performed. This new, multiple animal scanning technique could be particularly useful in studies

requiring a large number of animals to be imaged. Potential applications might include screening of transgenic mice that develop spontaneous tumours at variable latencies, evaluation of the biodistribution of short-lived tracers, particularly if alteration in specific activity may impact on the biological uptake, and therapeutic monitoring protocols involving several schedules and doses.

We have shown also that performing dynamic examinations of three mice simultaneously using shorter half-life positron emitters is feasible (Fig. 6). Here, sequential injection of ^{68}Ga-EDTA doses was performed by a single person within a 1.5-min period, since this was logistically more convenient than trying to inject three mice simultaneously. While results presented here relate to a tracer labelled with ^{68}Ga (68 min half-life), we expect that the same methodology can be applied using very short-lived

radioisotope labels, such as ^{11}C. Such radioisotopes were, however, not available in our laboratory at the time of this study. Nonetheless, new opportunities for studying TACs of multiple organs would arise from using short-lived isotopes. Improving the efficiency of establishing the absorption, distribution, metabolism and elimination (ADME) of drugs labelled with ^{11}C would be of potential benefit to drug development. As compared to static imaging, the gain in scanning throughput could be even more important with dynamic scanning, particularly when short half-time isotopes are used. More animals could be scanned with a given radiopharmaceutical dose, or the dose (or the number of syntheses) required to scan a sufficient number of animals to achieve a narrow confidence interval within the experimental design could be reduced, resulting in a more cost-effective use of short-lived tracers and animals.

Using clinical PET/CT imaging equipment the CT component of the combined system may offer several advantages. First, we employed CT-based attenuation correction. Visser et al. [10] observed a 40% difference between uncorrected and corrected image data in a mouse-sized phantom. Thus, attenuation correction is desirable in single rodent imaging and even more so when imaging several rodents simultaneously.

Second, the CT component of the PET/CT acquisitions may be particularly useful in better localizing tumour uptake in the case of abdominal disease (Fig. 5), when physiological uptake in the gastrointestinal tract of the mice may be confusing. In nude mice, which lack abdominal fat, image quality was poorer, especially in the case of haemorrhagic ascites (Fig. 3). The image quality of the CT part of the PET/CT acquisitions may be improved by the use of novel IV contrast media, but the optimal injection protocol has to be determined for each animal model and mouse strain [29]. Contrast media protocols including both IV and intraperitoneal injections would also improve CT image quality and tumour detection in the abdomen [30].

Despite the various advantages of using CT for attenuation correction and anatomical localization, attention has to be paid to the effective dose to the animal, which can be a limiting factor to repeat scans as part of longitudinal imaging sequences. This dose was 6.11 mGy computed tomography dose index (CTDI) per CT in our studies, which is lower than reported doses with dedicated small animal CT devices, ranging from 0.08 to 0.13 Gy [31, 32].

This study was not designed to compare a clinical PET/CT with a state-of-the-art DSA PET. Lately, new DSA PET systems have become commercially available and offer much improved image quality, sensitivity and quantitative accuracy [33–36]. While the spatial resolution obtained with PSF reconstruction in clinical PET/CT is on the order of 2 mm, thus being only slightly worse than that for DSA PET, there is no doubt that clinical PET/CT could not challenge DSA

PET in terms of sensitivity (Table 1). Moreover, PSF reconstruction or similar approaches could be used in DSA PET imaging [37]. Also, high-resolution clinical PET equipped with PSF reconstruction [38, 39] could be used to image small rodents. Finally, regarding large volume studies, it is noteworthy that the feasibility of imaging two rats simultaneously has been recently studied [40]. One might assume that imaging several mice simultaneously could be feasible on a large bore DSA PET, but has, to the best of our knowledge, not been reported so far.

Conclusion

This study shows that current clinical PET/CT systems, using advanced reconstruction algorithms that model the PSF of detector elements, can provide good quality images and accurate quantification of the radioactivity within pertinent sized lesions in tumour-bearing mice. Using these clinical PET systems multiple mice can be studied simultaneously in static and dynamic mode using attenuation correction routinely. Thus, state-of-the-art clinical PET/CT can be a practical option in experiments requiring high animal throughput and where DSA PET is not available.

Conflicts of interest None.

References

1. Nanni C, Di Leo K, Tonelli R, Pettinato C, Rubello D, Spinelli A, et al. FDG small animal PET permits early detection of malignant cells in a xenograft murine model. Eur J Nucl Med Mol Imaging 2007;34:755–62.
2. Aide N, Poulain L, Briand M, Dutoit S, Allouche S, Labiche A, et al. Early evaluation of the effects of chemotherapy with longitudinal FDG small-animal PET in human testicular cancer xenografts: early flare response does not reflect refractory disease. Eur J Nucl Med Mol Imaging 2009;36:396–405.
3. Dorow DS, Cullinane C, Conus N, Roselt P, Binns D, McCarthy TJ, et al. Multi-tracer small animal PET imaging of the tumour response to the novel pan-Erb-B inhibitor CI-1033. Eur J Nucl Med Mol Imaging 2006;33:441–52.
4. Wolf G, Abolmaali N. Imaging tumour-bearing animals using clinical scanners. Int J Radiat Biol 2009;85:752–62.
5. Panin VY, Kehren F, Michel C, Casey M. Fully 3-D PET reconstruction with system matrix derived from point source measurements. IEEE Trans Med Imaging 2006;25:907–21.

6. Pichler BJ, Wehrl HF, Judenhofer MS. Latest advances in molecular imaging instrumentation. J Nucl Med 2008;49(Suppl 2):5S–23S.

7. Townsend DW. Dual-modality imaging: combining anatomy and function. J Nucl Med 2008;49:938–55.

8. Huisman MC, Reder S, Weber AW, Ziegler SI, Schwaiger M. Performance evaluation of the Philips MOSAIC small animal PET scanner. Eur J Nucl Med Mol Imaging 2007;34:532–40.

9. Tatsumi M, Nakamoto Y, Traughber B, Marshall LT, Geschwind JF, Wahl RL. Initial experience in small animal tumor imaging with a clinical positron emission tomography/computed tomography scanner using 2-[F-18]fluoro-2-deoxy-D-glucose. Cancer Res 2003;63:6252–7.

10. Visser EP, Van Dalen JA, Laverman P, Newport D, Corstens FHM, Oyen WJG, et al. Evaluation of attenuation correction in the Inveon preclinical PET scanner using two opposite, rotating 57-Co sources. Eur J Nucl Med Mol Imaging 2007;34:S227.

11. Machulla HJ, Blocher A, Kuntzsch M, Piert M, Wei R, Grierson JR. Simplified labeling approach for synthesizing 3′-deoxy-3′-[18F]fluorothymidine ([18F]FLT). J Radioanal Nucl Chem 2000;243:843–46.

12. Zhernosekov KP, Filosofov DV, Baum RP, Aschoff P, Bihl H, Razbash AA, et al. Processing of generator-produced 68Ga for medical application. J Nucl Med 2007;48:1741–8.

13. Brambilla M, Secco C, Dominietto M, Matheoud R, Sachetti G, Inglese E. Performance characteristics obtained for a new 3-dimensional lutetium oxyorthosilicate-based whole-body PET/CT scanner with the National Electrical Manufacturers Association NU 2–2001 standard. J Nucl Med 2005;46:2083–91.

14. Daube-Witherspoon ME, Karp JS, Casey ME, DiFillipo FP, Hines H, Muehllehner G, et al. PET performance measurements using the NEMA NU-2001 standard. J Nucl Med 2002;43:1398–409.

15. Watson CC. New, faster, image-based scatter correction for 3-D PET. IEEE Trans Nucl Sci 2000;47:1587–94.

16. Kinahan PE, Hasegawa BH, Beyer T. X-ray-based attenuation correction for positron emission tomography/computed tomography scanners. Semin Nucl Med 2003;33:166–79.

17. Dinulescu DM, Ince TA, Quade BJ, Shafer SA, Crowley D, Jacks T. Role of K-ras and Pten in the development of mouse models of endometriosis and endometrioid ovarian cancer. Nat Med 2005;11:63–70.

18. Hoffman EJ, Huang SC, Phelps ME. Quantitation in positron emission computed tomography: 1. Effect of object size. J Comput Assist Tomogr 1979;3:299–308.

19. Soret M, Bacharach SL, Buvat I. Partial-volume effect in PET tumor imaging. J Nucl Med 2007;48:932–45.

20. Aide N, Louis MH, Dutoit S, Labiche A, Lemoisson E, Briand M, et al. Improvement of semi-quantitative small-animal PET data with recovery coefficients: a phantom and rat study. Nucl Med Commun 2007;28:813–22.

21. Bland JM, Altman DG. Statistical methods for assessing agreement between two methods of clinical measurement. Lancet 1986;1:307–10.

22. Hilson A. Bland-Altman plot. Radiology 2004;231:604. author reply 604–5.

23. Dandekar M, Tseng JR, Gambhir SS. Reproducibility of 18F-FDG microPET studies in mouse tumor xenografts. J Nucl Med 2007;48:602–7.

24. Nagengast WB, de Vries EG, Hospers GA, Mulder NH, de Jong JR, Hollema H, et al. In vivo VEGF imaging with radiolabeled bevacizumab in a human ovarian tumor xenograft. J Nucl Med 2007;48:1313–9.

25. Brix G, Doll J, Belleman ME, Trojan H, Haberkorn U, Schmidlin P, et al. Use of scanner characteristics in iterative image reconstruction for high-resolution positron emission tomography studies of small animals. Eur J Nucl Med 1997;24:779–86.

26. Seemann MD, Beck R, Ziegler S. In vivo tumor imaging using a state-of-the-art clinical PET/CT in comparison with a small animal PET and a small animal CT. Technol Cancer Res Treat 2006;5:537–42.

27. Aubry K, Shao Z, Monteil J, Paraf F, Bessède JP, Rigaud M. FDG-PET/CT of head and neck squamous cell carcinoma in a rat model. Mol Imaging Biol 2009;11:88–93.

28. Song SL, Liu JJ, Huang G, Wang ZH, Song YY, Sun XG, et al. Changes in 18F-FDG uptake within minutes after chemotherapy in a rabbit VX2 tumor model. J Nucl Med 2008;49:303–9.

29. Willekens I, Lahoutte T, Buls N, Vanhove C, Deklerck R, Bossuyt A, et al. Time-course of contrast enhancement in spleen and liver with Exia 160, Fenestra LC, and VC. Mol Imaging Biol 2009;11:128–35.

30. Aide N, Kinross K, Neels O, Roselt P, Hicks RJ. A dual contrast agent protocol improves 18F-FDG and 18F-FLT PET/CT imaging of mice bearing abdominal tumours. Eur J Nucl Med Mol Imaging 2009;36:S415.

31. Boone JM, Velazquez O, Cherry SR. Small-animal X-ray dose from micro-CT. Mol Imaging 2004;3:149–58.

32. Winkelmann CT, Figueroa SD, Rold TL, Volkert WA, Hoffman TJ. Microimaging characterization of a B16–F10 melanoma metastasis mouse model. Mol Imaging 2006;5:105–14.

33. Bao Q, Newport D, Chen M, Stout DB, Chatziioannou AF. Performance evaluation of the Inveon dedicated PET preclinical tomograph based on the NEMA NU-4 standards. J Nucl Med 2009;50:401–8.

34. Constantinescu CC, Mukherjee J. Performance evaluation of an Inveon PET preclinical scanner. Phys Med Biol 2009;54:2885–99.

35. Visser EP, Disselhorst JA, Brom M, Laverman P, Gotthardt M, Oyen WJ, et al. Spatial resolution and sensitivity of the Inveon small-animal PET scanner. J Nucl Med 2009;50:139–47.

36. Wang Y, Seidel J, Tsui BM, Vaquero JJ, Pomper MG. Performance evaluation of the GE Healthcare eXplore VISTA dual-ring small-animal PET scanner. J Nucl Med 2006;47:1891–900.

37. Qi J, Leahy RM, Cherry SR, Chatziioannou AF, Farquhar T. High-resolution 3D Bayesian image reconstruction using the microPET small-animal scanner. Phys Med Biol 1998;43:1001–13.

38. Sureau FC, Reader AJ, Comtat C, Leroy C, Ribeiro MJ, Buvat I, et al. Impact of image-space resolution modeling for studies with the high-resolution research tomograph. J Nucl Med 2008;49:1000–8.

39. Varrone A, Sjöholm N, Eriksson L, Gulyás B, Halldin C, Farde L. Advancement in PET quantification using 3D-OP-OSEM point spread function reconstruction with the HRRT. Eur J Nucl Med Mol Imaging 2009;36:1639–50.

40. Cheng TE, Yoder KK, Normandin MD, Risacher SL, Converse AK, Hampel JA, et al. A rat head holder for simultaneous scanning of two rats in small animal PET scanners: design, construction, feasibility testing and kinetic validation. J Neurosci Methods 2009;176:24–33.